

Real-Time GPS Precise Point Positioning-Based Precipitable Water Vapor Estimation for Rainfall Monitoring and Forecasting

Junbo Shi, Chaoqian Xu, Jiming Guo, and Yang Gao

Abstract—GPS-based precipitable water vapor (PWV) estimation has been proven as a cost-effective approach for numerical weather prediction. Most previous efforts focus on the performance evaluation of post-processed GPS-derived PWV estimates using International GNSS Service (IGS) satellite products with at least 3–9-h latency. However, the suggested timeliness for meteorological nowcasting is 5–30 min. Therefore, the latency has limited the GPS-based PWV estimation in real-time meteorological nowcasting. The limitation has been overcome since April 2013 when IGS released real-time GPS orbit and clock products. This becomes the focus of this paper, which investigates real-time GPS precise point positioning (PPP)-based PWV estimation and its potential for rainfall monitoring and forecasting. This paper first evaluates the accuracy of IGS CLK90 real-time orbit and clock products. Root-mean-square (RMS) errors of < 5 cm and ~ 0.6 ns are revealed for real-time orbit and clock products, respectively, during July 4–10, 2013. Second, the real-time GPS PPP-derived PWV values obtained at IGS station WUHN are compared with the post-processed counterparts. The RMS difference of 2.4 mm has been identified with a correlation coefficient of 0.99. Third, two case studies, including a severe rainfall event and a series of moderate rainfall events, have been presented. The agreement between the real-time GPS PPP-derived PWV and ground rainfall records indicates the feasibility of real-time GPS PPP-derived PWV for rainfall monitoring. Moreover, the significantly reduced latency demonstrates a promising perspective of real-time GPS PPP-based PWV estimation as an enhancement to existing forecasting systems for rainfall forecasting.

Index Terms—Precipitable water vapor (PWV), rainfall monitoring and forecasting, real-time orbit and clock correction, real-time precise point positioning (PPP).

I. INTRODUCTION

SINCE the introduction of global positioning system (GPS) meteorology in 1990s [1]–[4], GPS has been recognized as

Manuscript received January 29, 2014; revised July 9, 2014; accepted November 21, 2014. This work was supported in part by the National Key Developing Program for Basic Sciences of China under Grant 2012CB719902; by the National Natural Science Foundation of China under Grant 41371432; and by the Key Laboratory of Geospace Environment and Geodesy, Ministry of Education of China, under Grant 2013-2-2.

J. Shi, C. Xu, and J. Guo are with the School of Geodesy and Geomatics, Wuhan University, Wuhan 430079, China and also with the Key Laboratory of Precise Engineering and Industry Surveying, National Administration of Surveying, Mapping and Geoinformation, Wuhan 430079, China (e-mail: jbsshi@sgg.whu.edu.cn).

Y. Gao is with the Department of Geomatics Engineering, University of Calgary, Calgary, AB T2N 1N4, Canada.

Color versions of one or more of the figures in this paper are available online at <http://ieeexplore.ieee.org>.

Digital Object Identifier 10.1109/TGRS.2014.2377041

a cost-effective approach to determine precipitable water vapor (PWV) contents. Along with other meteorological sensors, GPS is able to provide PWV estimates with 1–3-mm root-mean-square (RMS) accuracy with respect to traditional atmosphere sensing techniques such as the radiosonde and the microwave radiometer (MWR) [5]–[10]. With the rapid deployment of GPS monitoring stations in local, regional, and global scales in recent years, ground-based GPS meteorology can offer much improved spatial and temporal resolutions for local or regional water vapor variations than the traditional techniques based on MWR and radiosonde observations.

Most GPS-based PWV systems to date rely on double-difference processing of GPS observations, e.g., Liou and Huang [11], Liou *et al.* [12], de Haan *et al.* [13], and Wang *et al.* [14]. There are some limitations for double-difference methods, such as they require the distance between GPS stations not less than 500 km and an absolute PWV value at one station in order to obtain the absolute PWV values at the other stations [3]. GPS PWV systems based on the processing of GPS undifferenced observations, known as precise point positioning (PPP), have been widely used in recent years since they can estimate absolute PWV with a single receiver [15]. Shoji [16] and Sato *et al.* [17] estimated PWV values based on the PPP technique using local and national GPS networks. Chiang *et al.* [18] and Choy *et al.* [19] utilized the GPS PPP-based PWV estimation approach to monitor typhoons and storms.

Although GPS PPP has the ability to provide high-precision PWV estimates, how to reduce the latency of GPS PPP-based PWV estimation remains a challenge. Several local and regional GPS networks have been employed to conduct near real-time PWV estimation using the International Global Navigation Satellite System (GNSS) Service (IGS) ultrarapid (IGU) orbit and clock products [16], [20]–[23]. However, the predicted IGU products suffer a latency of 3–9 h [24], which prevents the GPS PPP-based PWV estimation from real-time weather monitoring and nowcasting applications. To overcome the latency issue, IGS initiated the real-time pilot project with the infrastructure of real-time GNSS data streams on a global basis in 2007. After six years of experimental tests, IGS officially announced the real-time service (RTS) on April 1, 2013, which provides GPS real-time orbit and clock corrections to support real-time PPP at a global scale [25].

Most real-time PPP efforts so far are made with respect to positioning applications [26]–[31]. Limited work has been

reported on the use of real-time PPP for troposphere parameter estimation, particularly for weather forecasting applications. Liu and Li reported a PWV accuracy value of 2.2 mm using the predicted IGS orbits and the real-time clocks calculated by Wuhan University [32]. Pacione and Soehne compared zenith total delay (ZTD) estimates using IGS combined and individual orbit and clock corrections, respectively, and the ZTD consistency was identified [33]. Li *et al.* adopted the Helmholtz Centre Potsdam GeoForschungsZentrum's (GFZ) real-time orbit and clock corrections to conduct ambiguity-resolved PPP water vapor estimation with an accuracy value of 1.0–2.0 mm [34]. However, no efforts have been made to study the correlation between real-time GPS PPP-derived PWV values and the rainfall event. This becomes the focus of this paper, which investigates the potential of real-time GPS PPP-based PWV estimation using real-time orbit and clock products for rainfall monitoring. This paper will be organized as follows. Section II describes the mathematics for the real-time GPS PPP-based PWV estimation. Section III first carries out the accuracy assessment of the IGS CLK90 real-time orbit and clock products and then assesses the performance of real-time GPS PPP-derived PWV time series against the post-processed PWV time series. Two case studies, including a severe rainfall event in 2013 and a series of moderate rainfall events in 2014, are presented afterward. Finally, conclusions and future works are provided in Section IV.

II. PWV RETRIEVAL

The troposphere delay effect on GPS signals can be divided into a hydrostatic part and a wet part by

$$ZTD = ZHD + ZWD \quad (1)$$

where ZTD is the zenith total delay, ZHD is the zenith hydrostatic delay, and ZWD is the zenith wet delay.

The ZHD can be calculated as a function of the surface pressure P_0 , the geodetic latitude ϕ , and the geodetic height H by the Saastamoinen model as [35]

$$ZHD = \frac{(0.0022768 \pm 0.0000005)P_0}{1 - 0.00266 \cos(2\phi) - 0.00000028H}. \quad (2)$$

With the precise pressure data P_0 at the user location, the ZHD can be precisely calculated with up to 0.2-mm accuracy [36]. The necessary meteorological instruments, however, are not always installed at the user location. Thus, the global pressure and temperature (GPT) model is recommended to calculate the ZHD [37], [38].

On the contrary, there is no simple way to precisely model the ZWD. The usual approach is to estimate the ZWD in the PPP function model together with other parameters. In this paper, we use the PPP model developed by the University of Calgary

(UofC), which consists of three ionosphere-free observation combinations [39]

$$\frac{(P_1 + L_1)}{2} = \rho + c(dt^r - dt^s) + mf * ZWD - \lambda_1 \frac{N_1}{2} + \varepsilon_{\frac{(P_1+L_1)}{2}} \quad (3)$$

$$\frac{(P_2 + L_2)}{2} = \rho + c(dt^r - dt^s) + mf * ZWD - \lambda_2 \frac{N_2}{2} + \varepsilon_{\frac{(P_2+L_2)}{2}} \quad (4)$$

$$\begin{aligned} & \frac{f_1^2}{f_1^2 - f_2^2} L_1 + \frac{-f_2^2}{f_1^2 - f_2^2} L_2 \\ & = \rho + c(dt^r - dt^s) + mf * ZWD \\ & - \left(\frac{f_1^2}{f_1^2 - f_2^2} \lambda_1 N_1 + \frac{-f_2^2}{f_1^2 - f_2^2} \lambda_2 N_2 \right) + \varepsilon_{\frac{f_1^2}{f_1^2 - f_2^2} L_1 + \frac{-f_2^2}{f_1^2 - f_2^2} L_2} \end{aligned} \quad (5)$$

where $i = 1, 2$; P_i is the raw code measurement; L_i is the raw phase measurement; $f_1 = 154f_0$ and $f_2 = -154f_0$ with $f_0 = 10.23$ MHz; ρ is the geometric distance as a function of the receiver and satellite coordinates; c is the speed of light in vacuum; dt^r is the common receiver clock; dt^s is the common satellite clock; mf is the elevation-dependent mapping function of the ZWD; λ_i is the wavelength of carrier phase on frequency L_i ; N_i is the phase ambiguity on frequency L_i ; and ε contains residual errors, including multipath and noises.

PWV is related to ZWD via a conversion factor by

$$PWV = \Pi * ZWD \quad (6)$$

$$\Pi = \frac{10^6}{\rho_w R_v \left[\left(\frac{k_3}{T_m} \right) + k'_2 \right]} \quad (7)$$

where Π is the conversion factor; ρ_w is the density constant of liquid water; R_v is the gas constant for water vapor; k'_2 and k_3 are the atmospheric refractivity constants [2]; and T_m is the weighted mean temperature of the atmosphere.

T_m can be calculated using an integral formula with vapor pressure and temperature profile information along the zenith direction over the stations, which can be expressed as

$$T_m = \frac{\int (e/T) dz}{\int (e/T^2) dz} \quad (8)$$

where e is the vapor pressure, T is the absolute temperature, and dz is the integral path.

III. EXPERIMENT AND DISCUSSION

A. Real-Time Satellite Orbit and Clock Corrections

Currently, the IGS RTS provides combined orbit and clock corrections estimated in both single-epoch and Kalman filter approaches [40]. Moreover, several participating IGS agencies are also disseminating their own orbit and clock corrections for

various applications. For example, GFZ has been hosting a real-time PPP project with local reference network augmentation [41]; CNES has been developing a real-time zero-difference PPP integer ambiguity resolution demonstrator [29]. Therefore, real-time PPP users can choose the proper correction stream to match their specific application. This paper adopts the IGS CLK90 real-time correction stream from CNES because of its potential to support real-time PPP with integer ambiguity resolution.

As for the precise satellite orbits, coordinate vector r and velocity vector \dot{r} should be first calculated based on the broadcast ephemeris. The real-time orbit corrections encoded as the Radio Technical Commission for Maritime Services space-state representative (SSR) messages [42] are then applied by

$$r_{\text{SSR}} = r - [e_{\text{radial}} \quad e_{\text{along}} \quad e_{\text{cross}}] \delta O \quad (9)$$

where r_{SSR} is the corrected coordinate vector; $e_{\text{radial}} = \dot{r}/|\dot{r}|$; $e_{\text{along}} = (r \times \dot{r})/|r \times \dot{r}|$; $e_{\text{cross}} = e_{\text{radial}} \times e_{\text{along}}$; and δO is the SSR orbit correction vector in radial, along-track, and cross-track components.

As for the precise satellite clock error, the real-time clock correction equation is

$$dt_{\text{SSR}}^s = dt^s + \delta C/c \quad (10)$$

where dt_{SSR}^s is the corrected satellite clock error; $\delta C = C_0 + C_1(t - t_0) + C_2(t - t_0)^2$ is the clock correction; t is the broadcast clock time; t_0 is the reference time obtained from SSR clock correction messages; and C_0 , C_1 , and C_2 are three clock correction coefficients in the SSR clock correction messages.

The accuracy assessment of IGS CLK90 real-time orbit and clock products is conducted based on one-week consecutive corrections from July 4 to 10, 2013. IGS final orbit and clock products with nominal accuracy values of 2.5 cm and 0.075 ns, respectively, are selected as the reference. The orbit accuracy for each satellite is calculated as the RMS error of the differences between the real-time satellite coordinates and the reference coordinates. As to the clock accuracy, one reference satellite should be selected to make a single difference with the other satellites in order to remove the clock datum inconsistency between the real-time and final clock products. In this paper, the GPS satellite with pseudorandom noise (PRN) #1 is chosen as the reference satellite. The satellite clock accuracy is calculated as the RMS error of the differences between the real-time single-differenced clock errors and the reference clock errors.

Figs. 1 and 2 depict the accuracy values of the IGS CLK90 real-time orbits and clocks with respect to the IGS final products from July 4 to 10, 2013. A 3-D accuracy value of 4.82 cm is obtained for the real-time satellite orbits with accuracy values of 2.87/2.88/2.59 cm in XYZ directions, respectively. On the other hand, an overall accuracy value of 0.6 ns for the real-time satellite clock errors indicates that the IGS CLK90 real-time clock product can provide much better corrections than the IGS-predicted ultra-rapid clock product with a nominal accuracy value of ~ 3 ns (<http://igs.cb.jpl.nasa.gov/components/prods.html>).

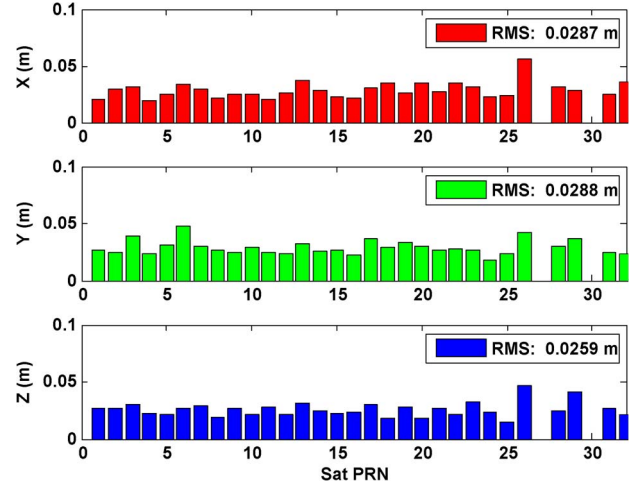


Fig. 1. Accuracy values of IGS CLK90 real-time orbit product with respect to IGS final orbit product from July 4 to 10, 2013.

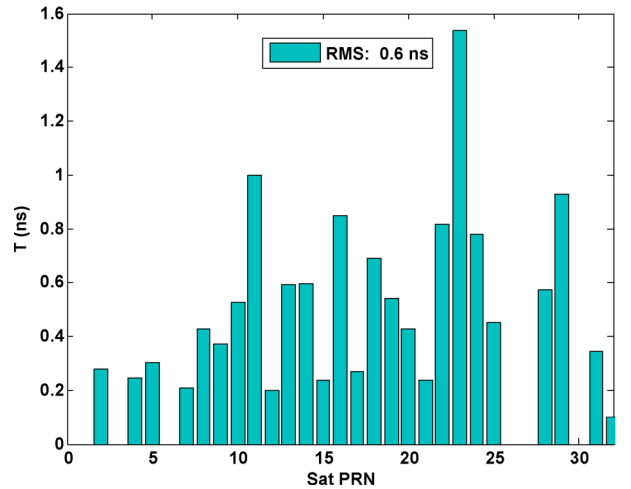


Fig. 2. Accuracy of IGS CLK90 real-time clock product with respect to IGS final clock product from July 4 to 10, 2013.

B. Comparison Between the Real-Time and Post-Processed GPS PPP-Derived PWV Time Series

In this section, the real-time GPS PPP-derived PWV time series are analyzed with respect to the PPP-derived PWV time series using the IGS final products. One-week GPS observations of IGS station WUHN collected at a sampling rate of 30 s from July 4 to 10, 2013, are processed. The PPP software package used is P3 developed by the UofC [43]. The elevation angle mask is set as 10° . The absolute phase center correction model is utilized to correct the antenna phase center offset and variation [44]. The pressure and temperature data are computed by the GPT model, and the ZHD is calculated using the Saastamoinen model. The troposphere mapping function is the global mapping function [45]. The ZWD is estimated in a random walk pattern with an initial standard deviation of 10^{-2} m and a spectral density of 10^{-6} m²/s. The factor for converting ZWD to PWV is calculated based on (7) with the mean weight temperature determined in [46].

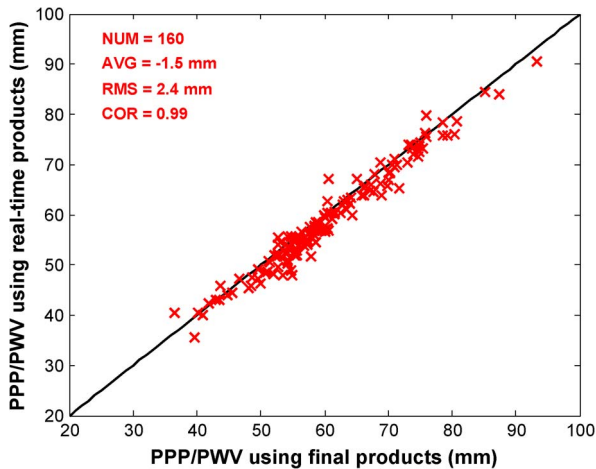


Fig. 3. Scatter plots of GPS PPP PWV series using real-time and final orbit and clock products. Number of elements (NUM), average value of PWV differences (AVG), RMS error of PWV differences, and correlation coefficient (COR) are included in the red-colored text.

The scatter plot of the PPP-derived PWV time series using real-time and final products is shown in Fig. 3. The PPP-derived PWV time series are resampled at the interval of 1 h, thus generating 168 PWV pairs during seven consecutive days. The average value and the RMS error are calculated for the PWV differences between the two PWV time series. The rule is applied to exclude PWV pairs with the difference larger than three-time RMS errors, which results in 160 PWV pairs for comparison. With respect to the PPP-derived PWV time series using IGS final products, the real-time PPP-derived PWV time series show an average value of -1.5 mm and an RMS error of 2.4 mm. On the other hand, the correlation coefficient of 0.99 is identified, which demonstrates that the real-time PPP-derived PWV time series have good consistency with the post-processed PPP-derived PWV series. Therefore, it is possible to use the real-time GPS PPP-derived PWV series for rainfall monitoring and forecasting.

C. Real-Time GPS PPP-Based PWV Estimation for Rainfall Monitoring and Forecasting: Case Studies

A severe rainfall event occurred in Wuhan, China, from July 5 to 7, 2013, which was regarded as the biggest rainfall event of this city in 2013. This rainfall event damaged 447.2 km² agricultural areas, and the economic loss was reported up to 250 million Chinese yuan [47]. It is therefore of great value to exploit the potential of real-time GPS PPP-based PWV estimation for rainfall monitoring and forecasting. A network consisting of 13 GPS stations around the city shown in Fig. 4 is employed in this paper. Five green rectangles represent GPS stations collocated with ground rainfall record instruments. The other nine stations without collocated rainfall records are marked as red triangles. The ground rainfall records are used to serve as the indicator of the rainfall forecasting by the real-time GPS PPP-based PWV estimation.

Figs. 5–9 depict the real-time PPP-derived PWV time series at the five GPS stations and the collocated ground rainfall records. The PPP-derived PWV time series demonstrate five

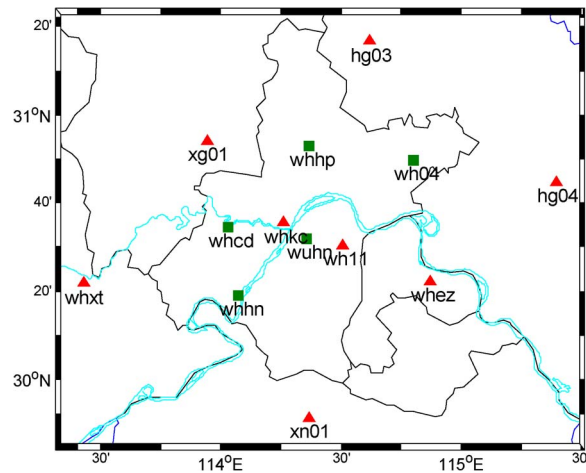


Fig. 4. Network of 13 GPS stations. Five stations marked as green rectangles are collocated with rainfall record instruments, whereas the other nine stations without rainfall records are marked as red triangles.

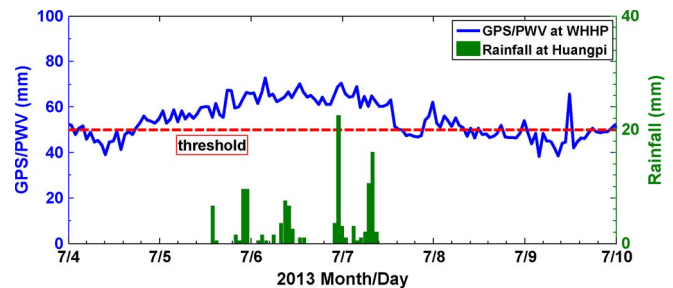


Fig. 5. Real-time GPS PPP-derived PWV time series at WHHP and the rainfall record at Huangpi during a heavy rainfall event in Wuhan from July 4 to 10, 2013.

stages corresponding to the different rainfall processes. First, the PPP-derived PWV time series fluctuate below 50 mm during the morning of July 4, one day before the rainfall. Second, the PPP-derived PWV estimates keep increasing from the noon of July 4 to the afternoon of July 5 during which period, the PPP-derived PWV values accumulate to ~ 60 mm. Third, the PPP-derived PWV series show an active variation pattern within the scope of 60–90 mm until the noon of July 7, whereas the rainfall amounts are observed by the ground record instruments. Fourth, the PPP-derived PWV time series dramatically decrease after the noon of July 7 while the rainfall stops. Fifth, the PPP-derived PWV time series fluctuate below the level of 50 mm after the noon of July 8 while no rainfall is recorded. Overall, the variations of the real-time GPS PPP-derived PWV time series are pretty consistent with the ground rainfall records.

Two facts should be noted for the comparison between the real-time GPS PPP-derived PWV series and the ground rainfall records. First, the threshold used in Figs. 5–9 is empirically set as 50 mm. As indicated in [12], the average PWV amount varies in different seasons; thus, it is improper to define a constant threshold for rainfall forecasting throughout the year. Instead, the threshold could be set as the average PWV amount of the clear days in the same period of past years. Second, the

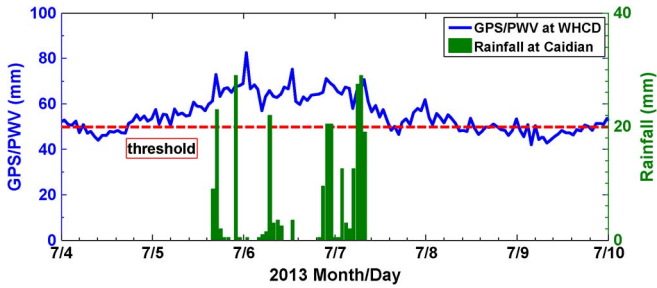


Fig. 6. Real-time GPS PPP-derived PWV time series at WHCD and the rainfall record at Caidian during a heavy rainfall event in Wuhan from July 4 to 10, 2013.

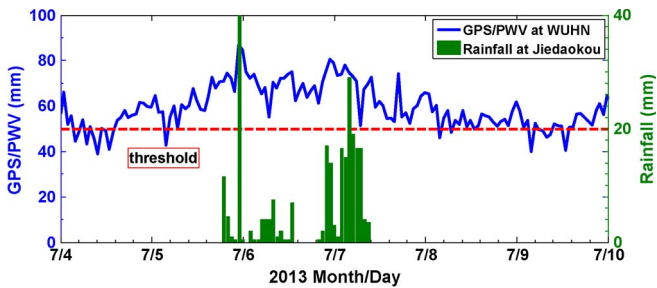


Fig. 7. Real-time GPS PPP-derived PWV time series at WUHN and the rainfall record at Jiedaokou during a heavy rainfall event in Wuhan from July 4 to 10, 2013.

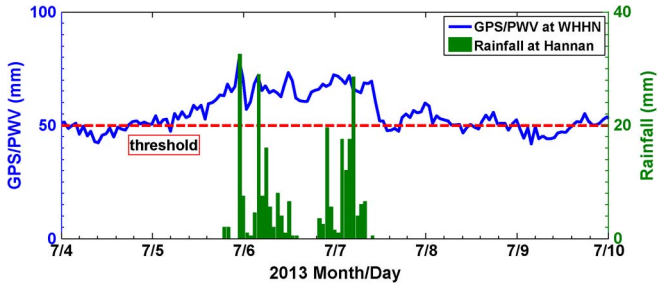


Fig. 8. Real-time GPS PPP-derived PWV time series at WHHN and the rainfall record at Hannan during a heavy rainfall event in Wuhan from July 4 to 10, 2013.

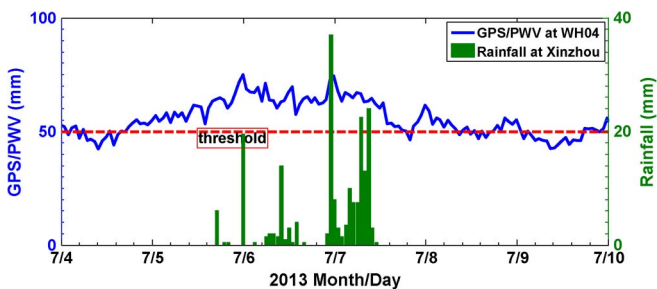


Fig. 9. Real-time GPS PPP-derived PWV time series at WH04 and the rainfall record at Xinzhou during a heavy rainfall event in Wuhan from July 4 to 10, 2013.

high PPP-derived PWV amount does not always indicate the occurrence of rainfall events. All the PPP-derived PWV time series in Figs. 5–9 show a high PWV level above 60 mm around

the midnight of July 8, but no rainfall amount is recorded during this period. This phenomenon can be also detected around the noon of July 9 at GPS station WHHP. In fact, the high PWV level is only one of the prerequisites of a rainfall event. Some external dynamic factors are also necessary to trigger a rainfall event. If the condition of external dynamic factors were not satisfied, the rainfall event might not happen even when the PPP-derived PWV estimates are at a high level.

GPS Continuously Operating Reference Station networks established worldwide and the IGS RTS have provided the infrastructure and necessary corrections for real-time GPS PPP, which enables real-time GPS PPP-based PWV estimation at global or regional scales. The analysis of the rainfall event in July 2013 has demonstrated the consistency between the real-time GPS PPP-derived PWV series and ground rainfall records. Furthermore, the continuously station-based PPP-derived PWV series can be also used to generate PWV maps to monitor PWV variation in real-time. A series of real-time PPP-derived PWV maps are depicted in Fig. 10 at the local time 00:00 during the pre-rain, the raining, and the post-rain periods, respectively. For better understanding, the animated PPP PWV maps at the interval of 1 h are available upon readers' request. Based on the network of 13 GPS stations, the real-time GPS PPP-derived PWV map can well reflect the PWV variation above the city of Wuhan.

A second case study concerns a series of moderate rainfall events at the same city during the period of April 15–21, 2014. Unlike the continuous rainfalls within two days in the first case, moderate rainfall events occurred every single day in the second case. We use a threshold of 40 mm to illustrate the consistency between real-time PPP-derived PWV series and ground rainfall records shown in Figs. 11–15. The ascending and descending patterns of real-time PPP-derived PWV series can be identified before and after each rainfall event. Meanwhile, the PWV fluctuation at a relatively stable level has been also detected during the raining stage. Overall, the real-time GPS PPP-derived PWV series match the ground rainfall records very well.

IV. CONCLUSION AND FUTURE WORK

This paper has investigated the performance of real-time GPS PPP-based PWV estimation and its potential for rainfall monitoring and forecasting with IGS CLK90 real-time orbit and clock. As regard the period of July 4–10, 2013, the orbit accuracy of < 5 cm and the clock accuracy of 0.6 ns have been identified for the IGS CLK90 real-time products. The corresponding real-time GPS PPP-derived PWV time series show an RMS error of 2.4 mm and a bias of -1.5 mm with respect to the post-processed GPS PPP-derived PWV time series using the IGS final products. Furthermore, a correlation coefficient of 0.99 is identified between the real-time and post-processed PPP-derived PWV time series based on one-week observations at IGS station WUHN.

The real-time GPS PPP-based PWV estimation has been applied to analyze a severe rainfall event in July 2013 and a series of moderate rainfall events in April 2014 at the city of Wuhan in China. The consistency between the real-time GPS PPP-derived PWV time series and the ground rainfall

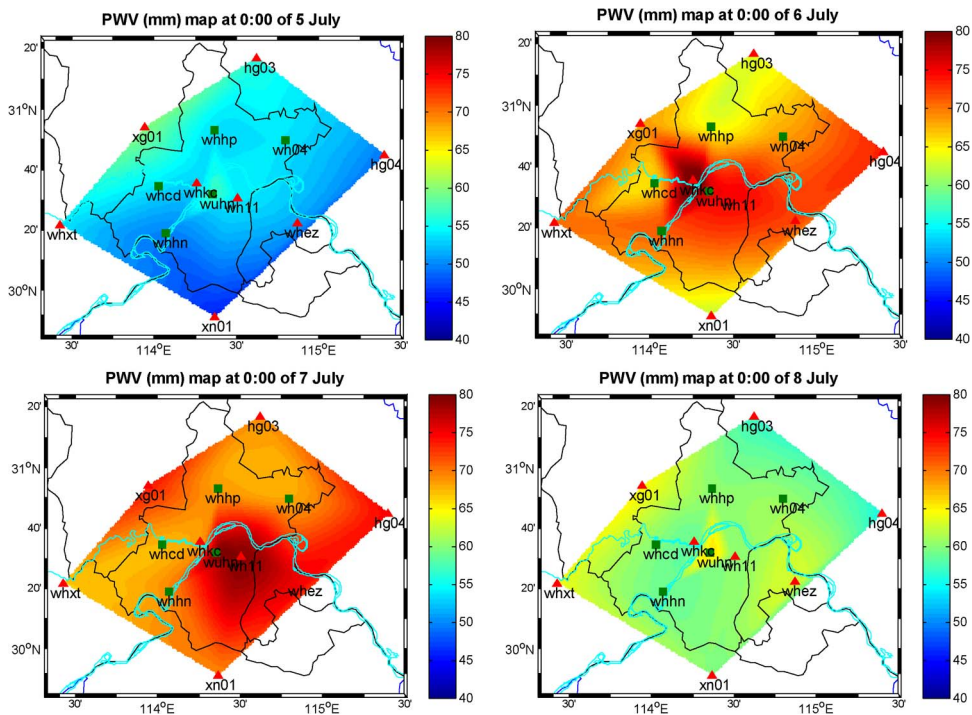


Fig. 10. Four real-time GPS PPP PWV maps at local time 00:00 in (top left, pre-rain) July 5, (top right, raining) July 6, (bottom left, raining) July 7, and (bottom right, post-rain) July 8, 2013.

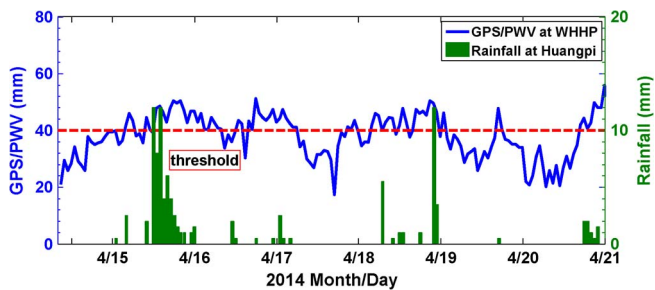


Fig. 11. Real-time GPS PPP-derived PWV time series at WHHP and the rainfall record at Huangpi during a series of moderate rainfall events in Wuhan from April 15 to 21, 2014.

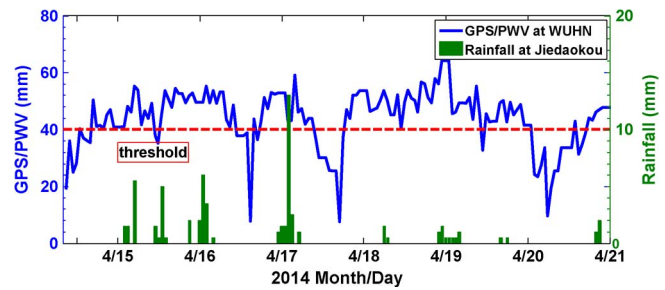


Fig. 13. Real-time GPS PPP-derived PWV time series at WUHN and the rainfall record at Jiedaokou during a series of moderate rainfall events in Wuhan from April 15 to 21, 2014.

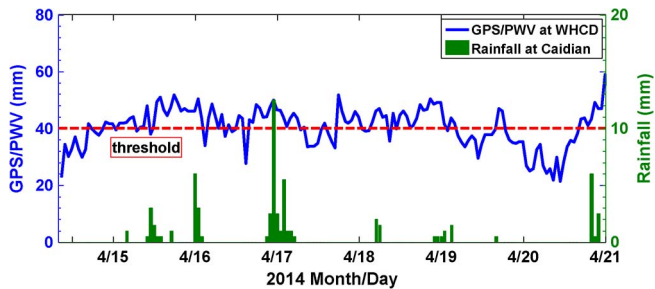


Fig. 12. Real-time GPS PPP-derived PWV time series at WHCD and the rainfall record at Caidian during a series of moderate rainfall events in Wuhan from April 15 to 21, 2014.

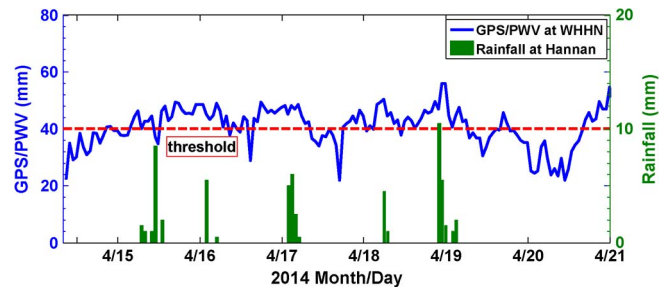


Fig. 14. Real-time GPS PPP-derived PWV time series at WHHN and the rainfall record at Hannan during a series of moderate rainfall events in Wuhan from April 15 to 21, 2014.

records verifies the feasibility of real-time PPP for rainfall monitoring and the potential for rainfall forecasting. Moreover, the real-time PPP-derived PWV map could be also utilized to better understand the temporal variations of water vapor content during severe weather conditions.

It should be noted that real-time GPS PPP cannot serve as a standalone system to forecast the occurrence of rainfall events. Some other dynamic factors that trigger the start of a rainfall event are also necessary. By introducing the real-time GPS PPP-derived PWV values into the existing assimilation and

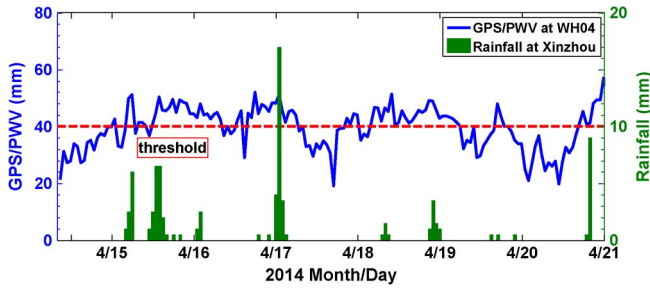


Fig. 15. Real-time GPS PPP-derived PWV time series at WH04 and the rainfall record at Xinzhou during a series of moderate rainfall events in Wuhan from April 15 to 21, 2014.

forecasting system, it is expected that the forecasting capability would be improved, particularly for short-term rainstorm warning.

ACKNOWLEDGMENT

The authors would like to thank IGS and CNES for providing the post-mission and real-time satellite precise orbit and clock products. They would also like to acknowledge the anonymous reviewers and the editor for their valuable comments on this manuscript.

REFERENCES

- [1] M. Bevis *et al.*, "GPS meteorology: Remote sensing of atmospheric water vapor using the global positioning system," *J. Geophys. Res.*, vol. 97, no. D14, pp. 15 787–15 801, Oct. 1992.
- [2] M. Bevis *et al.*, "GPS meteorology: Mapping zenith wet delays onto precipitable water," *J. Appl. Meteorol.*, vol. 33, no. 3, pp. 379–386, Mar. 1994.
- [3] J. Duan *et al.*, "GPS meteorology: Direct estimation of the absolute value of precipitable water," *J. Appl. Meteorol.*, vol. 35, no. 6, pp. 830–838, Jun. 1995.
- [4] C. Rocken *et al.*, "GPS/STORM-GPS sensing of atmospheric water vapor for meteorology," *J. Atmos. Ocean. Technol.*, vol. 12, no. 3, pp. 468–478, Jun. 1994.
- [5] D. E. Wolfe and S. I. Gutman, "Developing an operational, surface-based, GPS, water vapor observing system for NOAA: Network design and results," *J. Atmos. Ocean. Technol.*, vol. 17, no. 4, pp. 426–440, Apr. 2000.
- [6] J. Haase, M. Ge, H. Vedel, and E. Calais, "Accuracy and variability of GPS tropospheric delay measurements of water vapor in the western Mediterranean," *J. Appl. Meteorol.*, vol. 42, no. 11, pp. 1547–1568, Nov. 2003.
- [7] R. Pacione and F. Vespe, "GPS zenith total delay estimation in the Mediterranean area for climatological and meteorological applications," *J. Atmos. Ocean. Technol.*, vol. 20, no. 7, pp. 1034–1042, Jul. 2003.
- [8] J. Braun, C. Rocken, and J. Liljgren, "Comparisons of line-of-sight water vapor observations using the global positioning system and a pointing microwave radiometer," *J. Atmos. Ocean. Technol.*, vol. 20, no. 5, pp. 606–612, May 2003.
- [9] L. F. Sapucci, L. A. T. Machado, J. F. G. Monico, and A. P. Fattori, "Intercomparison of integrated water vapor estimates from multisensors in the Amazonian region," *J. Atmos. Ocean. Technol.*, vol. 24, no. 11, pp. 1880–1894, Nov. 2007.
- [10] S. Bonafoni *et al.*, "Assessment of water vapor retrievals from a GPS receiver network," *GPS Sol.*, vol. 17, no. 4, pp. 475–484, Oct. 2013.
- [11] Y. Liou and C. Huang, "GPS observations of PW during the passage of a typhoon," *Earth Planets Space*, vol. 52, no. 10, pp. 709–712, Oct. 2000.
- [12] Y. Liou, Y. Teng, T. V. Hove, and J. C. Liljgren, "Comparison of precipitable water observations in the near tropics by GPS, microwave radiometer, and radiosondes," *J. Appl. Meteorol.*, vol. 40, no. 1, pp. 5–15, Jan. 2001.
- [13] S. D. Haan, I. Holleman, and A. A. M. Holtslag, "Real-time water vapor maps from a GPS surface network: Construction, validation, and applications," *J. Appl. Meteorol. Climatol.*, vol. 48, no. 7, pp. 1302–1316, Jul. 2009.
- [14] H. Wang, M. Wei, G. Li, S. Zhou, and Q. Zeng, "Analysis of precipitable water vapor from GPS measurements in Chengdu region: Distribution and evolution characteristics in autumn," *Adv. Space Res.*, vol. 52, no. 4, pp. 656–667, Aug. 2013.
- [15] J. Zumberge, M. Heflin, D. Jefferson, M. Watkins, and F. Webb, "PPP for the efficient and robust analysis of GPS data from large networks," *J. Geophys. Res.*, vol. 102, no. B3, pp. 5005–5017, Mar. 1997.
- [16] Y. Shoji, "A study of near real-time water vapor analysis using a nationwide dense GPS network of Japan," *J. Meteorol. Soc. Jpn.*, vol. 87, no. 1, pp. 1–18, 2009.
- [17] K. Sato *et al.*, "A high-resolution, precipitable water vapor monitoring system using a dense network of GNSS receivers," *J. Disaster Res.*, vol. 8, no. 1, pp. 37–47, Feb. 2013.
- [18] K. Chiang, W. Peng, Y. Yeh, and K. Chen, "Study of alternative GPS network meteorological sensors in Taiwan: Case studies of the plum rains and Typhoon Sinlaku," *Sensors*, vol. 9, no. 6, pp. 5001–5021, Jun. 2009.
- [19] S. Choy, C. Wang, K. Zhang, and Y. Kuleshov, "GPS sensing of precipitable water vapour during the March 2010 Melbourne storm," *Adv. Space Res.*, vol. 52, no. 9, pp. 1688–1699, Nov. 2013.
- [20] J. V. Baelen, J. P. Aubagnac, and A. Dabas, "Comparison of near-real time estimates of integrated water vapor derived with GPS, radiosondes, and microwave radiometer," *J. Atmos. Ocean. Technol.*, vol. 22, no. 2, pp. 201–210, Feb. 2005.
- [21] R. Pacione and F. Vespe, "Comparative studies for the assessment of the quality of near-real-time GPS-derived atmospheric parameters," *J. Atmos. Ocean. Technol.*, vol. 25, no. 5, pp. 701–714, May 2008.
- [22] A. Karabatic, R. Weber, and T. Haiden, "Near real-time estimation of tropospheric water vapour content from ground based GNSS data and its potential contribution to weather now-casting in Austria," *Adv. Space Res.*, vol. 47, no. 10, pp. 1691–1703, May 2011.
- [23] C. Satirapod, S. Anonglekha, Y. Choi, and H. Lee, "Performance assessment of GPS-sensed precipitable water vapor using IGS ultra-rapid orbits: A preliminary study in Thailand," *Eng. J.*, vol. 15, no. 1, pp. 1–8, 2011.
- [24] J. Kouba, "A guide to using International GNSS Service (IGS) Products," Nat. Resour. Canada, Ottawa, ON, Canada, 2009. [Online]. Available: <http://acc.igs.org/UsingIGSProductsVer21.pdf>
- [25] M. Caissy, L. Agrotis, G. Weber, M. Hernandez-Pajares, and U. Hugentobler, *Coming Soon: The International GNSS Real-Time Service*, Auckland, New Zealand: GPS World, 2012. [Online]. Available: www.gpsworld.com/gnss-systemaugmentation-assistanceinnovation-coming-soon-13044/
- [26] Y. Altiner, L. Mervart, P. Neumaier, W. Sohne, and G. Weber, "Real-time PPP results from global orbit and clock corrections," presented at the EGU General Assembly, Vienna, Austria, May 6, 2010.
- [27] H. Li, J. Chen, J. Wang, C. Hu, and Z. Liu, "Network based real-time precise point positioning," *Adv. Space Res.*, vol. 46, no. 9, pp. 1218–1224, Nov. 2010.
- [28] D. Laurichesse, "The CNES real-time PPP with undifferenced integer ambiguity resolution demonstrator," in *Proc. ION GNSS*, Portland, OR, USA, Sep. 2011, pp. 654–662.
- [29] A. Sturze, L. Mervart, W. Sohne, G. Weber, and G. Wübbena, "Real-time PPP using open CORS networks and RTCM standards," presented at the PPP-RTK Symp., Frankfurt, Germany, 2012.
- [30] J. Chen *et al.*, "Performance of real-time precise point positioning," *Marine Geod.*, vol. 36, no. 1, pp. 98–108, Mar. 2013.
- [31] J. Shi, C. Xu, J. Guo, and Y. Gao, "Local troposphere augmentation for real-time precise point positioning," *Earth, Planets Space*, vol. 66, no. 30, p. 30, May 2014.
- [32] Z. Liu and M. Li, "The first PPP-based GPS water vapor real-time monitoring system in Pearl-River-Delta Region, China," in *Proc. CSNC*, 2013, pp. 71–87.
- [33] R. Pacione and W. Soehne, "Exploitation of the new IGS real-time products for GNSS meteorology," presented at the 4th Int. Galileo Science Colloq., Prague, Czech Republic, 2013.
- [34] X. Li *et al.*, "Real-time GPS sensing of atmospheric water vapor: Precise point positioning with orbit, clock and phase delay corrections," *Geophys. Res. Lett.*, vol. 41, no. 10, pp. 3615–3621, May 2014.
- [35] J. Saastamoinen, "Contributions to the theory of atmospheric refraction," *Bull. Géodésique*, vol. 105, no. 1, pp. 13–34, Sep. 1972.
- [36] S. Skone, "ENGO 633: Atmospheric effects on satellite navigation systems," Dept. Geomatics Eng., Univ. Calgary, Calgary, AB, Canada, Lecture notes, 2009.
- [37] J. Boehm, R. Heinkelmann, and H. Schuh, "Short note: A global model of pressure and temperature for geodetic applications," *J. Geod.*, vol. 81, no. 10, pp. 679–683, Oct. 2007.

- [38] P. Gérard and B. Luzum, IERS Conventions, 2010. [Online]. Available: <http://www.iers.org/iers/EN/Publications/TechnicalNotes/tn36.html?nn=94912>
- [39] Y. Gao and X. Shen, "A new method for carrier phase based precise point positioning," *Navig.—J. Inst. Navig.*, vol. 49, no. 2, pp. 109–116, Summer 2002.
- [40] IGS RTS, RTS Products, 2013. [Online]. Available: <http://rts.igs.org/products/>
- [41] X. Li, X. Zhang, and M. Ge, "Regional reference network augmented precise point positioning for instantaneous ambiguity resolution," *J. Geod.*, vol. 85, no. 3, pp. 151–158, Mar. 2011.
- [42] RTCM Special Committee 104, Differential GNSS (Global Navigation Satellite Systems) Services - Version 3 + Amendments 1, 2, 3, 4, and 5 to RTCM 10403.1, 2011. [Online]. Available: <https://ssl29.pair.com/dmarkle/puborder.php?show=3>
- [43] Y. Gao, P3 User Manual, 2005. [Online]. Available: http://people.ucalgary.ca/~ygao/p3_demo.htm
- [44] R. Schmid, How to Use IGS Antenna Phase Center Corrections. GPS World Tech Talk Blog, 2010. [Online]. Available: <http://www.gpsworld.com/tech-talk-blog/how-use-igs-antenna-phase-center-corrections-11369>
- [45] J. Boehm, A. Niell, P. Tregoning, and H. Schuh, "Global Mapping Function (GMF): A new empirical mapping function based on numerical weather model data," *Geophys. Res. Lett.*, vol. 33, no. 7, pp. L07304-1–L07304-4, Apr. 2006.
- [46] Y. Yao, C. Xu, B. Zhang, and N. Cao, "GTm-III: A new global empirical model for mapping zenith wet delays onto precipitable water vapor," *Geophys. J. Int.*, vol. 197, no. 3, pp. 202–212, Apr. 2014.
- [47] M. Yu, A News Report on the Severe Rainfall on 7 July, 2013 [Online]. Available: <http://www.weather.com.cn/news/2013/07/1914995.shtml>



Chaoqian Xu received the B.Sc. and M.Sc. degrees in geodesy and geomatics from Wuhan University, Wuhan, China, in 2011 and 2013, respectively, where he is currently working toward the Ph.D. degree in geodesy and surveying engineering in the School of Geodesy and Geomatics.

Currently, he is also with the Key Laboratory of Precise Engineering and Industry Surveying, National Administration of Surveying, Mapping and Geoinformation, Wuhan. His main research interests include Global Navigation Satellite System (GNSS)

data processing, global tropospheric modeling using multisource meteorology observations, and global ionospheric modeling based on GNSS observations.



Jiming Guo received the B.Sc. and M.Sc. degrees in engineering surveying from Wuhan Technical University of Surveying and Mapping, Wuhan, China, in 1985 and 1989, respectively, and the Ph.D. degree in geodesy and geomatics from Wuhan University, Wuhan, in 2001.

He is currently a Professor with Wuhan University. He is also with the Key Laboratory of Precise Engineering and Industry Surveying, National Administration of Surveying, Mapping and Geoinformation, Wuhan. His research interests include geodetic data

processing, high-precision Global Navigation Satellite System positioning technique, and applications.



Junbo Shi received the B.Sc. degree in geodesy and geomatics from Wuhan University, Wuhan, China, in 2005 and the Ph.D. degree in geomatics engineering from the University of Calgary, Calgary, AB, Canada, in 2012.

In 2010, he was a Research Engineer with Nexteq Navigation Corporation. He is currently a Lecturer with Wuhan University. He is also with the Key Laboratory of Precise Engineering and Industry Surveying, National Administration of Surveying, Mapping and Geoinformation, Wuhan. He has been the

author of more than 30 publications since 2007. His research interests include geomatics data processing, high-precision Global Navigation Satellite System (GNSS) positioning, GNSS-based troposphere/ionosphere modeling, and GNSS meteorology.

Dr. Shi was a member of The Institute of Navigation, the Canadian Geophysical Union, and the Chinese Professionals in Global Positioning Systems.



Yang Gao received the B.Sc. and M.Sc. degrees in surveying engineering from Wuhan University, Wuhan, China, in 1982 and 1985, respectively, and the Ph.D. degree in geomatics engineering from the University of Calgary, Calgary, AB, Canada, in 1992.

He is currently a Professor with the University of Calgary. Prior to joining the University of Calgary in 1998, he held positions as a Research Scientist, a Manager of GPS Research & Development, and a Manager of Asia-Pacific in the private sector. He has published more than 250 papers and has received a

number of awards for his contributions to the field. His research interests focus on high-precision Global Navigation Satellite System (GNSS) and multisensor navigation systems.

Dr. Gao is a Fellow of the International Association of Geodesy (IAG), the Chairman of the IAG Sub-Commission 4.5 "High Precision GNSS Algorithms and Applications," and an Editor of several journals.